Ultrafast and Highly Sensitive Photodetectors Fabricated on High-Energy-Nitrogen–Implanted GaAs

An ion-implantation technique has been employed in the GaAs photodetector technology to obtain materials with a carrier lifetime in the picosecond and even subpicosecond regimes. Properties of proton,[1] Ar^+,[2,3] As^+,[4–6] and other ion-implanted GaAs have been investigated thoroughly. Nitrogen-ion–implanted GaAs (N^+-GaAs) is a relatively new member in the family of ion-implanted GaAs materials. The implantation of nitrogen into GaAs was initially done to get a diluted ternary semiconductor GaAsN. Optical properties of GaAsN, such as photoluminescence[7] and N^+-induced band-gap reduction,[8] have been studied. It was also noted that high-energy implantation of N^+ ions produced a highly resistive material after high-temperature annealing.[9] The aim of this article is to present the preparation and properties of metal–semiconductor–metal (MSM) photodetectors fabricated on high-energy-N^+–implanted GaAs and demonstrate the performance improvement of these devices, as compared with those fabricated on low-temperature (LT)-grown GaAs.

We prepared the N^+-GaAs material by implanting N^+ ions with an energy E_{impl} of 700 keV and 880 keV, respectively, into 2-μm-thick, *n*-doped GaAs films grown by molecular beam epitaxy (MBE) on semi-insulating GaAs (001) substrates with resistivity $>10^7$ Ω cm at 300 K. The implantation was performed in a linear, 900-kV accelerator,[10] and the ion dose was 3×10^{12} cm^{-2}. Figure 95.47 shows the implantation profiles of N^+ ions in GaAs, calculated using the TRIM (transport of ions in matter) simulation program.[11] TRIM is the most widely used software to calculate the stopping and range of ions in matter. We note that for samples implanted with E_{impl} = 700 keV and 880 keV, the N^+ ions reached a depth of 1250 nm and 1400 nm, respectively. Thus, in both cases, there is a thin nonimplanted layer of *n*-doped GaAs. This layer is expected to affect properties of our devices at very high bias voltages; it should not, however, influence our photoresponse measurements since the penetration depth of 810-nm photons is approximately 1 μm. In future devices, the contribution from the nonimplanted region, where the carrier lifetime is much longer and mobility much higher, could be minimized by implanting GaAs with higher energies and higher doses.

MSM structures, 10 μm wide and 20 μm long, with a finger width of 1 μm and finger spacing of 1.5 μm, were patterned on our two types of N^+-GaAs materials, using conventional photolithography and a lift-off technique. The MSM devices consisted of Ti/Au contacts with a thickness of 10/160 nm. Next, the surfaces of our structures, except for the MSM area, were coated with 200 nm of SiO_2 to provide electrical insulation, and the external Ti/Au coplanar strip (CPS) lines with a thickness of 50/600 nm, needed for electrical measurements, were fabricated. To compare performance, several photodetectors with identical MSM geometries were also fabricated on LT-GaAs grown by MBE on semi-insulating GaAs substrates.

Figure 95.48 presents typical current–voltage (*I–V*) characteristics of both the N^+-GaAs and LT-GaAs photodetectors measured in the dark at 300 K. The N^+-GaAs devices exhibit

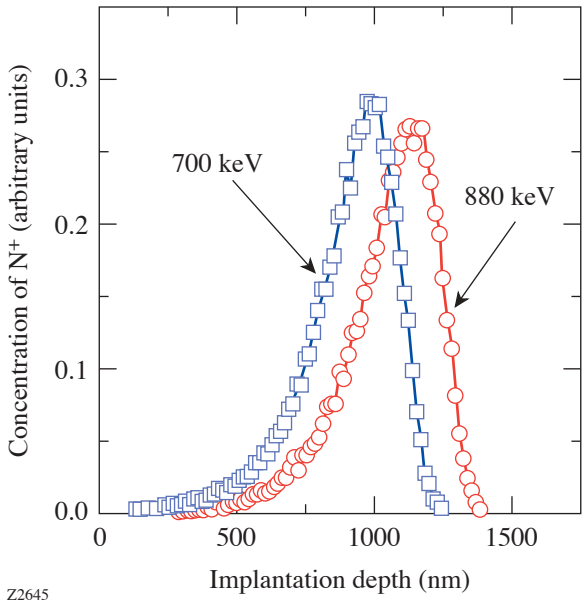

Figure 95.47
TRIM-simulated profiles of the penetration depth of implanted N^+ ions into an *n*-doped GaAs film. Squares correspond to E_{impl} = 700-keV GaAs and circles to E_{impl} = 880 keV.

ohmic dependence up to a voltage bias $V_B \approx 6$ V and a quadratic dependence at higher biases. V_B up to 25 V and 32 V was applied to the 700-keV and 880-keV N^+-GaAs MSM's, respectively, with no dielectric breakdown occurring. The rapid increase of the dark current at the highest V_B's for our N^+-GaAs photodetectors can be explained by carriers collected from the device's deep, nonimplanted region, where the conductivity is much higher. Note that the transition to the nonlinear part of the *I–V* occurs for the 880-keV device at somewhat higher V_B than that for the 700-keV N^+-GaAs MSM, in accordance with the N^+ implantation profiles shown in Fig. 95.47. As expected, the LT-GaAs structures show ohmic behavior in the entire range of applied V_B (30 V max, corresponding to an average electric field of 200 kV/cm). However, their actual dark currents are significantly higher, especially at low V_B (<10 V), where the best performer, N^+-GaAs MSM with E_{impl} = 880 keV, exhibits the lowest (below 10 nA) dark current.

Figure 95.49 shows the current responsivity of our N^+-GaAs and LT-GaAs photodetectors versus the MSM bias. The devices were illuminated with continuous, 855-nm radiation from a laser diode. The beam spot was approximately equal to the MSM active area, and the optical power incident on the photodetector was P_{in} = 100 μW. The responsivity was obtained by dividing the induced photocurrent (total current minus the dark current) by P_{in}. In comparison to the LT-GaAs device, our highly implanted N^+-GaAs photodetector exhibited more than two times higher responsivity. At the very high bias, we observed in both of our N^+-GaAs MSM's a drastic increase in the responsivity, which can be attributed to the partial penetration of 855-nm photons deeply into our structures and the collection of photocarriers from the nonimplanted regions of our devices.

All time-resolved photoresponse studies of our N^+-GaAs and LT-GaAs devices were performed using 100-fs-wide, 810-nm-wavelength, 82-MHz-repetition rate optical pulses from a commercial Ti:sapphire laser. The photoresponse waveforms of our devices were recorded with the help of our electro-optic (EO) sampling system, using a total-internal-reflection $LiTaO_3$ microprobe, and featuring ~200-fs temporal resolution.[12] The electrical transients were sampled at a spot on the CPS lines located approximately 30 μm away from the photodetectors. The time-resolved photoresponse waveforms of our devices are shown in Fig. 95.50. Under the same

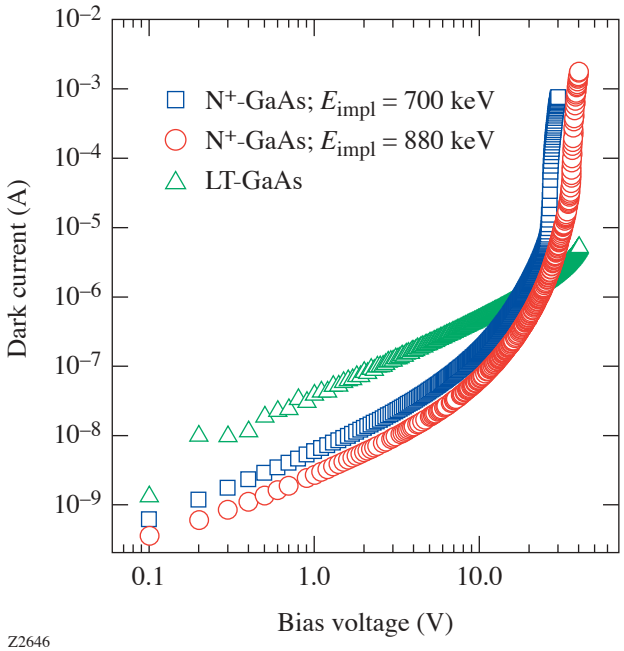

Figure 95.48
Dark *I–V* characteristics of the MSM photodetectors, fabricated on 700-keV N^+-GaAs (squares), 880-keV N^+-GaAs (circles), and LT-GaAs (triangles), respectively.

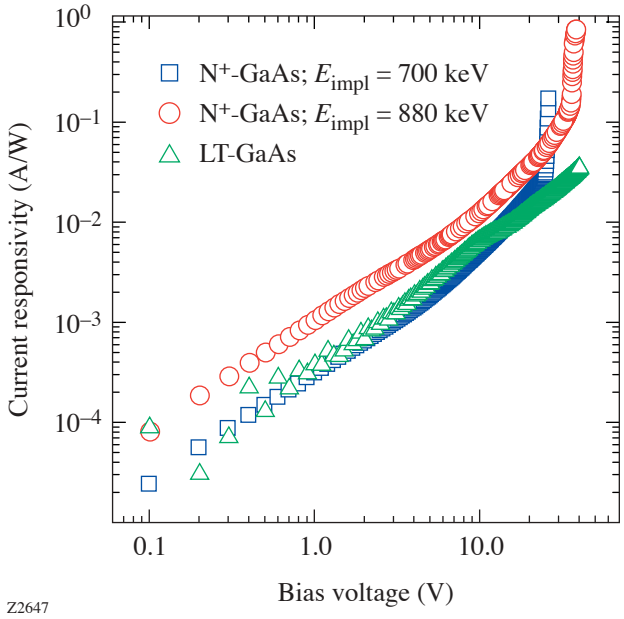

Figure 95.49
Current responsivity of the three tested MSM photodetectors as a function of the bias voltage.

operating conditions, all of our photodetectors exhibited transients with the same 10%–90% risetime of 700 fs and the exponential falling edge with a $1/e$ decay time of ~2.5 ps. While the rise time is due to the 30-μm distance between the MSM and the probe beam spot, the 2.5-ps-long exponential pulse decay shows that the photoresponse dynamics is not limited by the subpicosecond carrier lifetime in either N^+-GaAs or LT-GaAs, but corresponds to the capacitance of the MSM structure. Indeed, the calculated capacitive time constant[13] of our photodetectors is 2.1 ps, in excellent agreement with the decay time of the transients shown in Fig. 95.50.

We note that superior responsivity of N^+-GaAs devices translates into their high sensitivity. For E_{impl} = 880 keV, the N^+-GaAs photodetector exhibits a signal peak amplitude as high as 2 V, when biased at 9 V and illuminated by an incident optical power, P_{in} = 12 mW. This amplitude value is more than 50% higher than that for our best LT-GaAs photodetector operated under the same conditions. Figure 95.51 presents the photoresponse amplitudes of the photoresponse transients of the three photodetectors as a function of P_{in}, with V_B = 9 V. We observe that all dependences are initially linear and gradually approach saturation. As we showed in Fig. 95.50, the photoresponse amplitudes of N^+-GaAs devices are significantly higher than the amplitude of the LT-GaAs device. They also start to saturate at significantly higher P_{in} values, looking almost linear within our tested range.

In conclusion, we have fabricated novel photodetectors based on high-energy-nitrogen–implanted GaAs. These devices show very low dark currents at low-voltage bias. These currents are almost two orders of magnitude lower than those in the best-known, commercially implemented LT-GaAs devices. Simultaneously, the current responsivity of our N^+-GaAs photodetectors is significantly higher, as compared to LT-GaAs structures. The N^+-GaAs devices also exhibit excellent sensitivity, with the 880-keV, N^+-GaAs photodetector being the best performer. The latter photodetector has a peak photoresponse amplitude of up to 2 V. Under the illumination of 100-fs-wide and 810-nm-wavelength laser pulses, all tested photodetectors exhibited an ~2.5-ps-wide photoresponse, limited by the MSM capacitive time constant. Our research shows that N^+-GaAs photodetectors are very promising as highly sensitive photodetectors for high-speed applications, and they represent a cheaper alternative to LT-GaAs devices. The performance of N^+-implanted GaAs photodetectors can be further improved by increasing the implantation depth, using higher E_{impl} and larger N^+ doses.

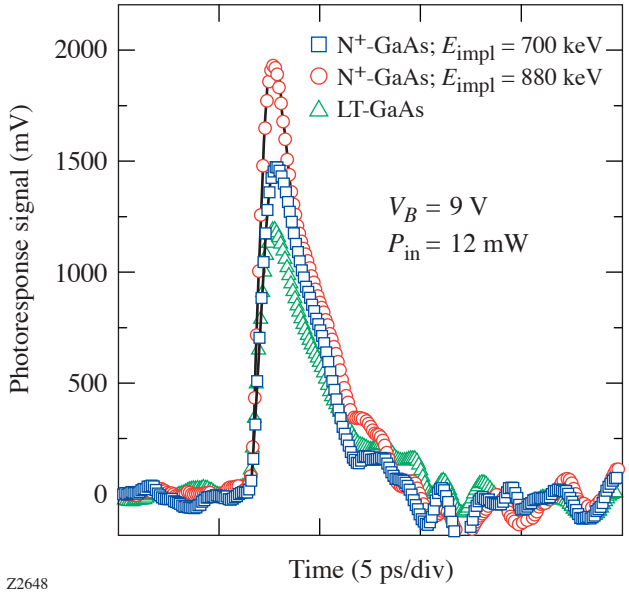

Figure 95.50
Transient photoresponse signals of the three tested MSM photodetectors, excited by 100-fs-wide, 810-nm optical pulses and recorded using the EO sampling system.

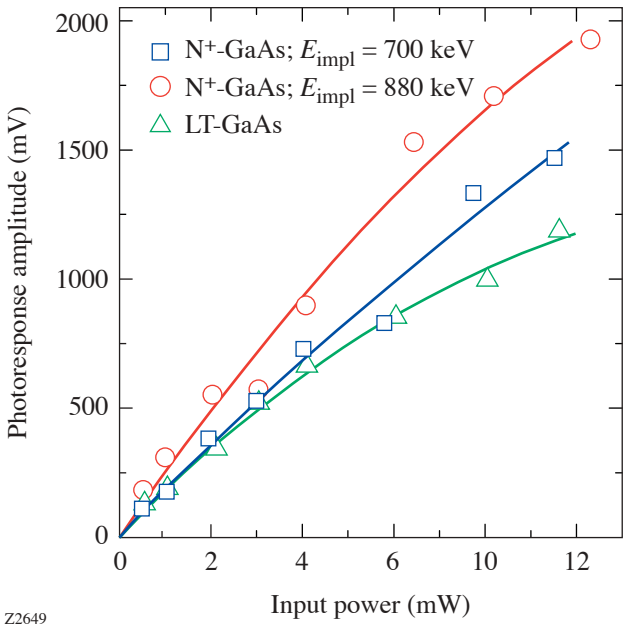

Figure 95.51
Photoresponse amplitudes of the photoresponse transients (Fig. 95.50) as a function of the bias voltage for the three tested MSM photodetectors. The solid lines are guides to the eye.

ACKNOWLEDGMENT

This work was supported by the National Science Foundation Grant INT-0078949 and by Corning Inc. Additional support was provided by NYSTAR through the Center for Electronic Imaging Systems at the University of Rochester.

REFERENCES

1. M. Lambsdorff *et al.*, Appl. Phys. Lett. **58**, 1881 (1991).
2. A. A. Kutas *et al.*, Mater. Sci. Eng. B **B34**, 32 (1995).
3. B. Breeger *et al.*, Nucl. Instrum. Methods Phys. Res. B **161**, 415 (2000).
4. A. Claverie, F. Namavar, and Z. Lilental-Weber, Appl. Phys. Lett. **62**, 1271 (1993).
5. F. Ganikhanov *et al.*, Appl. Phys. Lett. **67**, 3465 (1995).
6. H. Fujioka *et al.*, J. Appl. Phys. **78**, 1470 (1995).
7. X. Weng *et al.*, J. Appl. Phys. **92**, 4012 (2002).
8. W. Shan *et al.*, Appl. Phys. Lett. **75**, 1410 (1999).
9. J. F. Chen *et al.*, Appl. Phys. Lett. **76**, 2283 (2000).
10. P. Kováč, M. Pavlovič, and J. Dobrovodsky, Nucl. Instrum. Methods Phys. Res. B **B85**, 749 (1994).
11. J. F. Ziegler, J. P. Biersack, and U. Littmark, *The Stopping and Range of Ions in Solids*, The Stopping and Ranges of Ions of Matter, Vol. 1 (Pergamon Press, New York, 1985); see also http://www.srim.org/.
12. X. Zheng, Y. Xu, R. Sobolewski, R. Adam, M. Mikulics, M. Siegel, and P. Kordoš, Appl. Opt. **42**, 1726 (2003).
13. Y. C. Lim and R. A. Moore, IEEE Trans. Electron Devices **ED-15**, 173 (1968).